Global Optimization of Multimodal Aerodynamic Optimization Benchmark Case

D.J. Poole *, C.B. Allen †, T.C.S. Rendall‡

Department of Aerospace Engineering, University of Bristol, Bristol, BS8 1TR, U.K.

An investigation into a multimodal aerodynamic optimization benchmark case using an approximate global optimization approach is presented. A new benchmark case of the AIAA Aerodynamic Design Optimization Discussion Group that involves the drag minimization of a rectangular NACA0012 wing subject to lift and root bending moment, as well as other geometric constraints, that is currently believed to be multimodal has been suggested. In this paper, optimization of that case using a constrained population-based global optimization framework is presented, with three independent runs of the optimizer (each with different starting locations) having been performed. The runs are all coarsely-converged to give approximately converged solutions such that rapid run-times can be achieved and used to demonstrate any pitfalls that may be encountered when using a gradient-based optimizer. All three of the runs converged onto drag values close to the theoretical optimum, however with substantially different final shapes. This likely indicates the presence of a flat optimum region within the design space, where a substantial number of wing shapes are able to obtain the theoretical optimum span loading.

I. Introduction and Background

Aerodynamic shape optimization (ASO) is the process used to optimize a given aerodynamic shape within a computational environment to improve on a design requirement. The aerodynamic model (normally a computational fluid dynamics (CFD) flow solver) is used to evaluate some metric against which to optimize called the objective, which in the case of ASO is an aerodynamic quantity, such as drag [1] or range [2], subject to a set of constraints which are usually aerodynamic or geometric. Along with the fluid flow model, the ASO framework requires a surface parameterization scheme which mathematically describes the aerodynamic shape being optimized by a series of design variables; changes in the design variables, which are made by a numerical optimization algorithm, result in changes in the aerodynamic surface. Numerous advanced optimizations using compressible computational fluid dynamics (CFD) as the aerodynamic model have previously been performed [3–7]. The authors have also presented work in this area, having developed a modularised, generic optimization tool, that is flow solver and mesh type independent, and applicable to any aerodynamic problem [8, 9].

A substantial amount of research has been published for a number of decades in the field of ASO; review-like works have been presented in parameterization [10], and optimizer performance [11, 12]. One primary issue on the development of the research field has been a lack of consistent benchmarking of individual ASO frameworks on unified test cases. As such, the AIAA Aerodynamic Design Optimization Discussion Group (ADODG)[a] was formed. As part of this, a number of inviscid and viscous aerofoil and wing optimization cases were suggested, with a number of research groups presenting results; see [13–20] for example.

Recently, a new benchmark case has been suggested. The case involves the drag reduction of a rectangular NACA0012 wing subject to a substantial number of aerodynamic and geometric constraints [21]. The primary reason for introducing this new problem is to investigate a benchmark case that appears to exhibit multimodality, which is defined as a problem that has more than one local minimum, knowledge of which

*Graduate Student. Email: d.j.poole@bristol.ac.uk

†Professor of Computational Aerodynamics. Email: c.b.allen@bristol.ac.uk

‡Lecturer. Email: thomas.rendall@bristol.ac.uk

[a] https://info.aiaa.org/tac/ASG/APATC/AeroDesignOpt-DG/default.aspx

is extrememly important as the degree of multimodality has a substantial implication on the choice of optimization algorithm. The most common type of optimization algorithm employed when solving ASO problems is a gradient-based approach, where the local sensitivities of the objective and constraints with respect to the design variables are used as a basis to construct a search direction. In the case of a unimodal problem (where there is a single optimum solution), a gradient-based method will terminate at the single optimum. On the other hand, in the presence of a multimodal problem, the gradient-based algorithm will terminate at the nearest local optimum along which the initial search direction drives it. Hence, the major problem is that termination of a gradient-based method is guaranteed to find a minimum, but there is no knowledge of whether this is the global minimum or a local minimum. If a global optimum is known to be needed, then a global optimization approach can be used. Global optimization methods are typically either evolutionary algorithms (EAs), such as genetic algorithms (GA)[22] or differential evolution (DE)[23, 24], or swarm intelligence algorithms (SIAs), such as particle swarm optimization (PSO)[25], ant colony optimisation [26] or gravitational search algorithm [27]. Typically these use a population of individuals who evolve or cooperate together in pursuit of the global optimum, which, while being ideal for global optimization, comes at the cost of a substantial increase in the number of CFD flow solutions required [28].

The degree of multimodality in the field of aerodynamic shape optimisation is, somewhat, an unknown question, and very problem dependent. Often the test of local or global minima is by comparing the final results of a gradient-based optimisation against global optimisation for the same case, and that if the results are different, then the logical explanation is that multiple local minima exist. This conclusion is, by nature, predicated on the fact that the local optimiser has successfully converged and has not just exited due to errors (often associated with either the inability to accurately compute gradients, or difficulties in convergence of the flow solver). If local optimisation results have successfully converged, then in the event of differing results for comparison between gradient-based and global search optimisers, the modality must be due to either the parameterisation or the flow solution. For aerofoil optimization, it has been suggested that ASO problems exist that are unimodal [11] and multimodal[29, 30], while the same is true of wings exhibiting unimodality [6] and multimodality [11]. Furthermore, recently, aerodynamic topology optimization results have suggested multimodality for a number of supersonic flow problems [31].

Due to the substantial cost of using a global optimization approach for an ASO problem, and the apparent lack on multimodality in a number of ASO problems, global optimizers have had only a small use in ASO, see[32–36] for example. However, to tackle the ADODG multimodal benchmark problem, ideally a global optimizer should be employed. As such, in this work, the benchmark problem is tackled using a state-of-the-art constrained global optimization framework [37]. The framework, which uses uses a parallel decomposition of the search agent population for efficient computation, has previously been used for drag minimization of aerofoils [1] and is used here for the wing optimization. An approximate approach to global optimization is performed using coarse-convergence to investigate the practicalities of this problem without the higher cost associated with fully converging a global optimizer.

The remainder of the paper is organised as follows: in sections II and III, the optimization problem and ASO framework are outlined, respectively; results are presented in section IV; finally, conclusions are given in section V.

II. Problem Definition

In this section, the overall problem is described. First, a generic form of a constrained optimization problem is given, followed by the aerodynamic optimization problem considered,

II.A. Constrained Optimization Problem Definition

A generic single-objective optimization problem optimizes an objective function, J, which is a function of a vector of D design variables, $\boldsymbol{\alpha}$, subject to a set of inequality, $\mathbf{g}$, and equality, $\mathbf{h}$, constraints. Bound constraints are also included for completion, which state that the design variables must lie within the D-orthotope bounded region in $\Re^D$, called the design space, $\mathcal{S}$. Bound constraints can also be written as $\mathbf{L} \leq \boldsymbol{\alpha} \leq \mathbf{U}$ where $\mathbf{L}$ and $\mathbf{U}$ are D-long vectors and give the lower and upper bounds of the design space, outside of which, $J(\boldsymbol{\alpha})$ has an unknown solution. Commonly this type of problem is known as a constrained

numerical optimization problem (CNOP), which formally, is written as:

$$\begin{aligned} \underset{\boldsymbol{\alpha}\in\Re^D}{\text{minimise}} \quad & J(\boldsymbol{\alpha}) \\ \text{subject to} \quad & \mathbf{g}(\boldsymbol{\alpha}) \leq \mathbf{0} \\ & \mathbf{h}(\boldsymbol{\alpha}) = \mathbf{0} \\ & \boldsymbol{\alpha} \in \mathcal{S} \end{aligned} \tag{1}$$

The solution to a CNOP is the global optimum solution, $\boldsymbol{\alpha}^*$, that minimises the objective function:

$$J(\boldsymbol{\alpha}^*) \leq J(\boldsymbol{\alpha}) \ , \forall \boldsymbol{\alpha} \in \mathcal{F}$$

where $\mathcal{F}$ is the feasible region, which is the region in $\mathcal{S}$ where all the constraints are satisfied.

II.B. Aerodynamic Problem Definition

The aerodynamic optimization problem requires the drag minimization of a rectangular NACA0012 wing of full aspect ratio 6 (without wing-cap). The wing is composed of a rectangular NACA0012 section of span 3.0 and a rounded wing-cap of width 0.06, resulting in the overall semi-span of 3.06. The wing is in compressible, inviscid flow at $M_\infty = 0.5$ and is trimmed to a target $C_L = 0.2625$.

The objective is drag minimization subject to aerodynamic constraints on lift C_L, and root bending moment, C_{M_x}, and geometric constraints on wing area, S, internal volume, V, twist, γ, local chord, $c(y)$, local thickness, $t(y)$, sweep (local x deformation at the quarter-chord), $\Delta x_{qc}(y)$, semi-span, s, dihedral (local z deformation at the quarter chord), $\Delta z_{qc}(y)$, and angle of attack, θ. The problem is given by:

$$\begin{aligned} \underset{\boldsymbol{\alpha}\in\Re^D}{\text{minimise}} \quad & C_D \\ \text{subject to} \quad & C_L = 0.2625 \\ & C_{M_x} \leq 0.1069 \\ & S = S(\text{initial}) \\ & V \geq V(\text{initial}) \\ & -3.12^\circ \leq \gamma \leq 3.12^\circ \\ & 0.45 \leq c(y) \leq 1.55 \quad \forall y \in [0, s] \\ & 0.06 \leq t(y) \leq 0.18 \quad \forall y \in [0, s] \\ & -1 \leq \Delta x_{qc}(y) \leq 1 \quad \forall y \in [0, s] \\ & 2.46 \leq s \leq 3.67 \\ & -0.45 \leq \Delta z_{qc}(y) \leq 0.45 \quad \forall y \in [0, s] \\ & -3.0^\circ \leq \theta \leq 6.0^\circ \end{aligned} \tag{2}$$

III. Optimization Framework

In this section, the overall optimization framework used for performing the aerodynamic optimizations outlined later is described. A global optimization approach (as opposed to a gradient-based approach) with a reduced set of design parameters is considered. The flow solver and mesh, geometry and mesh control scheme, and optimizer are described individually below.

III.A. Flow Solver and Mesh

The flow-solver used is a structured multiblock, finite-volume, unsteady, cell-centred scheme solving the compressible Euler equations in cartesian and rotating coordinate system. The convective terms are evaluated using the Jameson-Schmidt-Turkel (JST) scheme [38], chosen such that numerical drag is minimised. Multi-stage Runge-Kutta with local timestepping is used for time integration, and convergence acceleration is achieved through V- and W-cycle multigrid [39].

A 666,000 cell, eight-block structured C-mesh was generated [40]; 129× 41 surface mesh, 33 points on either side of the wake, and 41 points between the inner and outer boundary. Figure 1 shows domain and boundaries, farfield mesh, and two views of the surface mesh and chordwise planes.

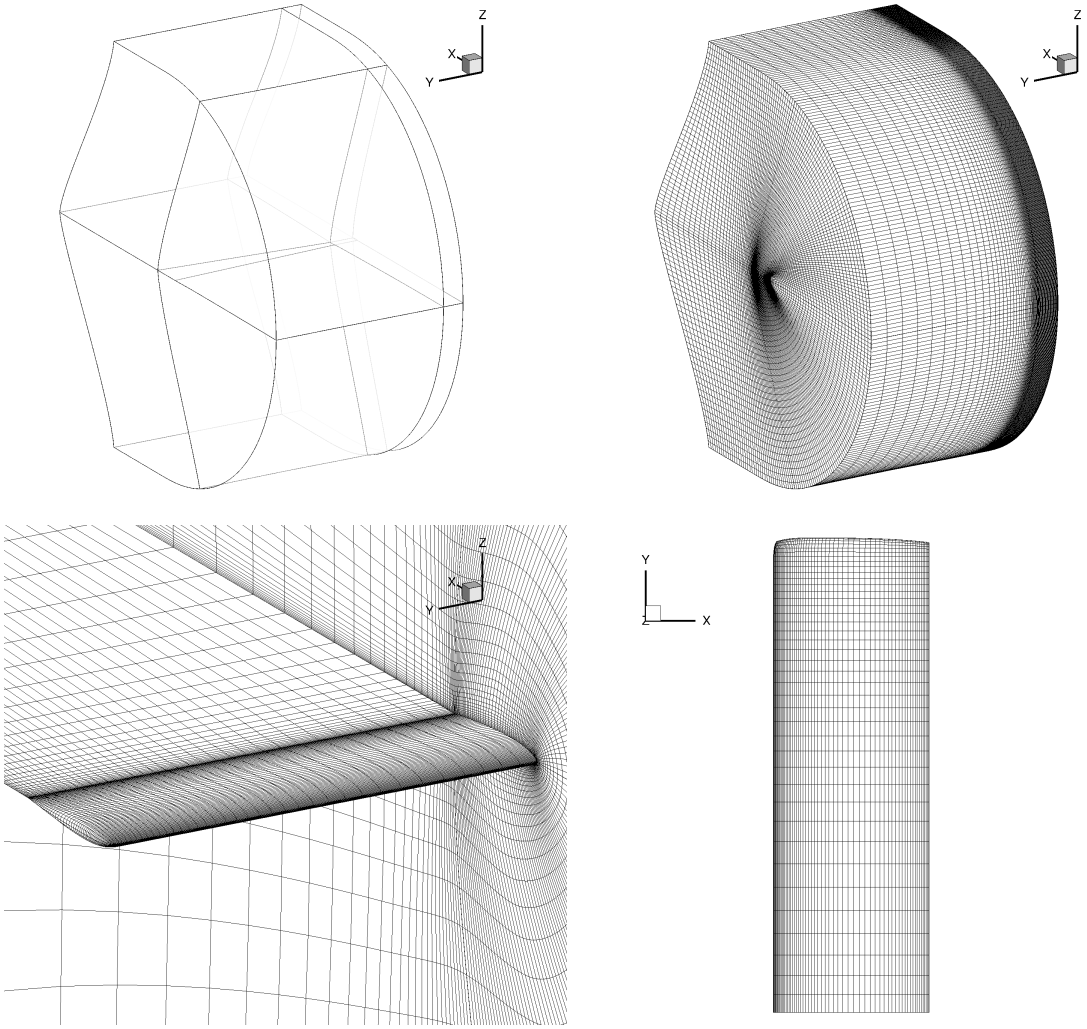

Figure 1: Eight-block wing mesh

III.B. Shape Control

The geometry and mesh control scheme must be flexible enough to allow sufficient design space investigation and efficient enough to maximise design space coverage with a minimum number of design parameters. The consideration of a global optimization approach necessitates the requirement for a minimum number of design variables to reduce computational burden as much as possible. The design variables used are primarily planform changes, which are from a mix of global planform deformation and local, sectional planform changes. Before describing the design variables, it is first necessary to describe the unified surface control and mesh deformation scheme.

For suitable surface control and mesh deformation, an efficient domain element shape parameterization method has been developed by the authors and presented previously for CFD-based shape optimization [8, 41]. The parameterization technique, surface control and volume mesh deformation all use radial basis functions (RBFs), wherein global interpolation is used to provide direct control of the design surface and the CFD mesh, which is deformed in a high-quality fashion [42, 43].

Setting up an RBF interpolation, $s(\mathbf{x})$, through a set of n data points, $\mathcal{X}$, where $\mathbf{x}_i \in \mathcal{X} \quad \forall i \in [1, \ldots, n]$

where the function to be modelled, $f(\mathbf{x})$, is known, which at the i-th data point has a scalar value, f_i, where $\mathbf{x}$ is a vector of inputs in a d-dimensional space, $\mathbf{x} = \{x^{(1)}, \ldots, x^{(d)}\}$. For a chosen basis function, ϕ, which is a function of the Euclidean distance, $\|\cdot\|$, between two vectors, the interpolation takes the form:

$$s(\mathbf{x}) = \sum_{i=1}^{n} \beta_i \phi(\|\mathbf{x} - \mathbf{x}_i\|) \tag{3}$$

where the coefficients, $\boldsymbol{\beta}$, are found by solving a linear system, $\mathbf{f} = \mathbf{M}\boldsymbol{\beta}$, constructed using the known data points to provide exact recovery of the data at the sites; hence $\mathbf{M}$ is a matrix of basis functions evaluated between the known sites.

When using RBF interpolation for unified shape control and mesh deformation, the known data sites are a small set of nc control points, where the i-th control point has a location in Cartesian space given by $\mathbf{x}_{c_i} = [x_{c_i}, y_{c_i}, z_{c_i}]$ which are commonly placed either close to or on the aerodynamic surface to give detailed control. Deformation of the control points leads to deformation of the mesh according to the RBF system, hence combinations of control point deformations act as design variables. Furthermore, the basis function in question is the radially-decaying Wendland C^2 [44] function, where the influence of the function is controlled by the support radius, outside of which the influence is zero.

For this work, to ensure smooth spanwise deformations, a hierarchical approach to constructing the design variables is achieved [45]. The overall set-up of control points and design variables is given in figure 2. A number of global deformations are combined with local deformations at a small number of spanwise locations, with a blending function used to blend intermediate deformations between the spanwise locations. There are therefore two levels of control points; driver (which controls the deformation) and passenger (which acts to create smooth spanwise deformations). For this work, 24 driver control points at five equally spaced spanwise stations are employed for the higher level, while 24 passenger control points at four equally spaced spanwise stations between each of the higher level sections are used for the lower level. This leads to a total of 21 spanwise stations, each with 24 control points, all arranged in a lattice structure.

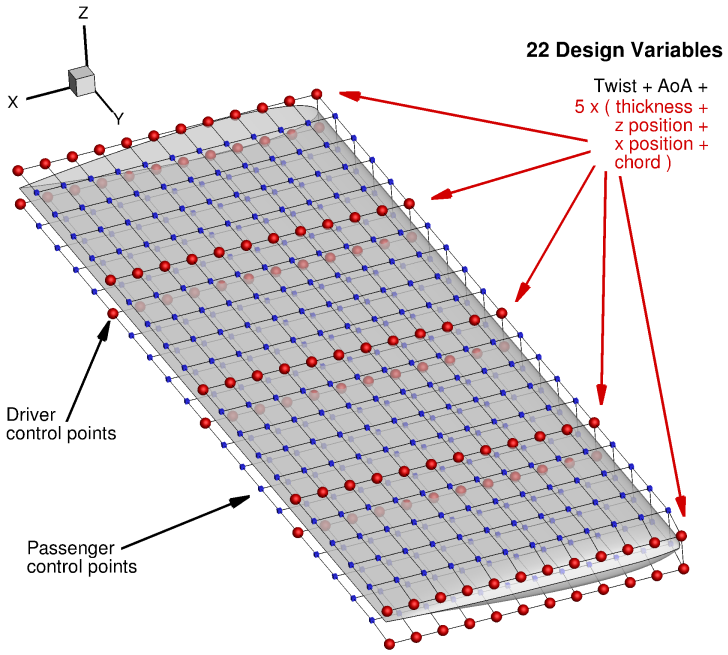

Figure 2: Hierarchical control points

The design variables are constructed to maintain maximum flexibility, while restricting the dimensionality which otherwise causes a global optimizer to have convergence issues. One global geometric design variable is used, which is linear twist. Local sectional geometric design variables for the driver control points are thickness, vertical deformation (to create dihedral), chordwise deformation (to create sweep) and chord. Span is allowed to vary, however this is not directly controlled by the optimizer, and instead it is calculated

to ensure the wing area constraint is maintained. Angle of attack is also allowed to vary within the limits set by the constraint. This leads to a total of 22 design variables.

Deformations of the passenger control points are determined using the driver control points either side of a passenger's spanwise station. The passenger deformation is therefore a partition of unity blending between the deformations at the preceding and succeeding driver spanwise station. Using a partition of unity blending has the advantage of first, being able to recover global deformations (such as a global thickness change) from local deformations, and second, providing smooth spanwise blending between a small set of driver control points. Figure 3 shows an example of an increase in the local chord on the second driver spanwise station with no other changes versus adding a decrease in the local chord on the third spanwise station, clearly showing the positive blending that is occurring to ensure a smooth chord distribution.

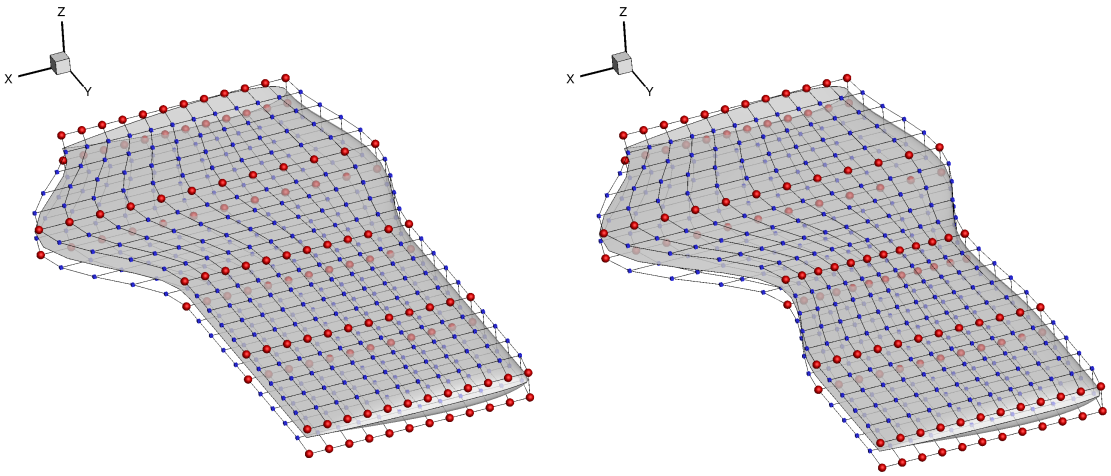

(a) Positive (b) Positive and negative

Figure 3: Chord change design variables

III.C. Optimizer

A global optimization approach is considered here, as opposed to a gradient-based approach. While global optimization can often be more expensive than performing gradient-based optimization, it is more likely to locate a globally optimal solution in a multimodal design space. Due to performing three-dimensional optimization, the run-time of the objective function evaluation, which is a CFD flow solve, is considerably higher than two-dimensional optimization (which the authors have previously performed [1]). To this end, approximate global optimization is performed to give trends in the design space, where the population-based algorithm used here is coarsely-converged. This involves running for a smaller number of iterations than would be required for full convergence, allowing a more rapid run-time while still giving indicative results.

The global optimization algorithm used is an agent-based method, where a population of agents are used to traverse the design space in search of a solution. The location of the n-th agent (which is an individual within a population of N agents) within the search space of D design variables is $\boldsymbol{\alpha}_n = [\alpha_n^{(1)}, \alpha_n^{(2)}, \ldots, \alpha_n^{(D)}]^T$, and in an agent-based optimization algorithm moves to a new location, in the d-th dimension, at the next iteration of the search by:

$$\alpha_n^{(d)} = \alpha_n^{(d)} + v_n^{(d)} \tag{4}$$

where $\mathbf{v}_n$ is the vector of location deformations, which is more commonly termed a particle's velocity, the determination of which separates various agent-based method.

A hybrid of the particle swarm optimization (PSO) [25], and the gravitational search algorithm (GSA) [27] has been developed and used here such that the memory qualities of PSO complement the global transfer of data that occurs in GSA to obtain a highly efficient global search algorithm. Furthermore, the design space exploration capabilities of PSO are combines with the optima exploitation capabilities of GSA to provide an

algorithm that can both explore the design space and exploit the global optimum within it. The velocity of particles is calculated as:

$$v_n^{(d)} = r_n v_n^{(d)} + a_n^{(d)} \tag{5}$$

where r_n is a uniformly distributed random number on the interval $[0, 1]$, and $\mathbf{a}_n$ is the particle's 'acceleration', which is a blend of PSO and GSA components:

$$a_n^{(d)} = W a_n^{(d)}(\text{pso}) + (1 - W) a_n^{(d)}(\text{gsa}) \tag{6}$$

where $\mathbf{a}_n(\text{pso})$ and $\mathbf{a}_n(\text{gsa})$ are the PSO and GSA constituents of the acceleration respectively, and W is a blending constant used to balance the qualities of PSO and GSA. Setting $W = 1$ means the search is driven by only PSO, while setting $W = 0$ means the search is driven by only GSA. To obtain a good balance, 0.5 is used in this work. The acceleration due to PSO is:

$$a_n^{(d)}(\text{pso}) = c_1 r_{1_n}(p_n^{(d)} - \alpha_n^{(d)}) + c_2 r_{2_n}(s^{(d)} - \alpha_n^{(d)}) \tag{7}$$

where c_1 is the cognitive constant, c_2 is the social constant, r_{1_n} and r_{2_n} are independent uniformly distributed random numbers on the interval $[0, 1]$, $\mathbf{p}_n$ is the individual's best location found so far, and $\mathbf{s}$ is the global (swarm's) best location found so far. The acceleration due to GSA is given as:

$$a_n^{(d)}(\text{gsa}) = F_n^{(d)} / M_n \tag{8}$$

where $\mathbf{F}_n$ is the forcing vector calculated using Newtonian mechanics and M_n is the particle mass, which is proportional to the fitness of the particle relative to all other particles (particles with a low objective function have a high mass and *vice versa*). A comparison of the update approaches between PSO and GSA is given in figure 4.

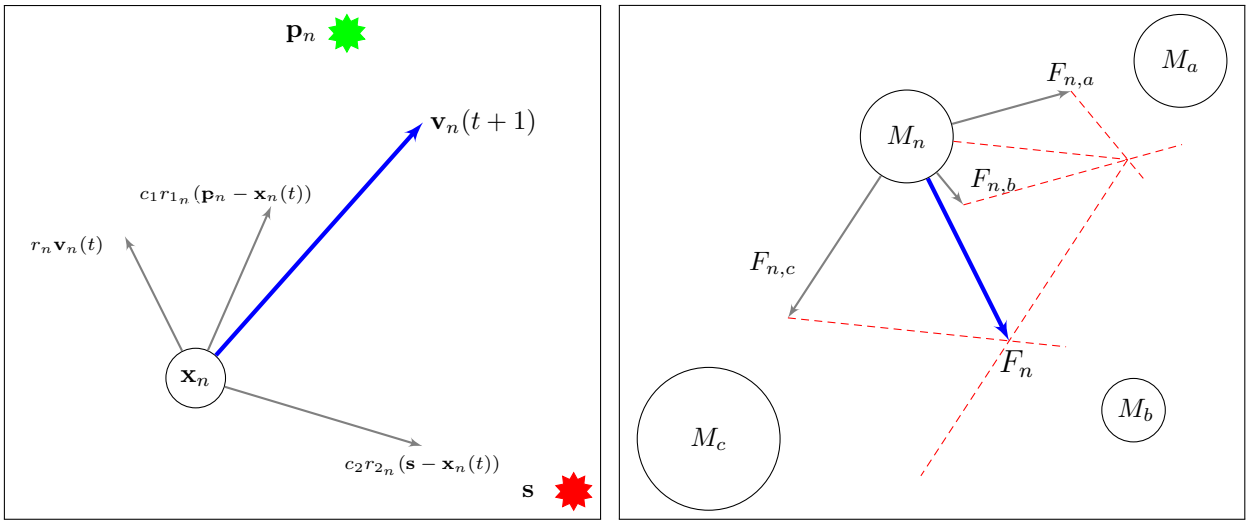

(a) PSO (b) GSA

Figure 4: Comparison of PSO and GSA update frameworks.

Constraints are not directly handled in the PSO or GSA algorithms, hence the separation-sub-swarm (3S) [37] constraint handling method is applied. The 3S method is a constraint handling framework that can be applied to any swarm intelligence algorithm and works by splitting the overall population into two independent swarms every iteration – one swarm containing all of the feasible particles at that iteration (all constraints are satisfied) and one containing all of the infeasible particles at that iteration (at least one constraint is violated). The swarms then independently solve a different objective function, where the objective function of a particle ζ is determined by:

$$\zeta(\boldsymbol{\alpha}) = \begin{cases} J(\boldsymbol{\alpha}) & \text{if } \lambda(\boldsymbol{\alpha}) = 0 \\ \lambda(\boldsymbol{\alpha}) & \text{else} \end{cases} \tag{9}$$

where λ is the sum of the constraint violations. Hence, the infeasible particles have the objective of minimizing the constraint violation and therefore trying to find the feasible region whereas the feasible particles are minimizing the objective that is to be solved for. Updates to the swarm's and an individual's best location are performed using a binary tournament selection [46], which is achieved via the domination operator; given two locations within the design space, $\boldsymbol{\alpha}_a$ and $\boldsymbol{\alpha}_b$:

$$\boldsymbol{\alpha}_b \mapsto \boldsymbol{\alpha}_a \Leftrightarrow \boldsymbol{\alpha}_a \prec \boldsymbol{\alpha}_b \tag{10}$$

where

$$\boldsymbol{\alpha}_a \prec \boldsymbol{\alpha}_b \Leftrightarrow \begin{cases} J(\boldsymbol{\alpha}_b) < J(\boldsymbol{\alpha}_a) \text{ and } \lambda(\boldsymbol{\alpha}_a), \lambda(\boldsymbol{\alpha}_b) \leq 0 \\ \lambda(\boldsymbol{\alpha}_b) \leq 0 \text{ and } \lambda(\boldsymbol{\alpha}_a) > 0 \\ \lambda(\boldsymbol{\alpha}_b) < \lambda(\boldsymbol{\alpha}_a) \text{ and } \lambda(\boldsymbol{\alpha}_a), \lambda(\boldsymbol{\alpha}_b) > 0 \end{cases} \tag{11}$$

Bound constraints are handled by placing a particle back in its previous position if it violates the bound constraints i.e. is outside the design space.

The 3S algorithm has been shown to outperform other common constraint handling methods such as penalty methods [37]. The overall framework has also successfully been applied to inviscid and viscous aerofoil optimization [1].

III.D. Optimization Problem Definition

The aerodynamic problem definition has previously been outlined, however, the problem definition that the optimizer deals with is slightly different. The reason for these differences is due to the way the design variables have been constructed. For example, explicit local and global planform changes are specified by design variables, hence, to avoid the over-specification of the problem (too many constraints), many of the linear constraints outlined in equation 2 can be converted to bound constraints. This improves performance of the optimizer.

Before the optimization problem can be fully described, the design variable specification needs to be explained. The design variable specification is as follows:

- α_1 - angle of attack
- α_2 - linear twist
- α_3 to α_7 - thickness changes of each section of driver control points
- α_8 to α_{12} - z-deformation of each section of driver control points
- α_{13} to α_{17} - x-deformation of each section of driver control points
- α_{18} to α_{22} - chord changes of each section of driver control points

As noted above, the span is calculated after the planform deformation to ensure the projected area constraint is satisfied. Also, to give the optimizer full flexibility, the lift constraint is implemented as an inequality constraint with the angle of attack variable. In previous work by the authors [1] on aerofoil drag minimization, using this approach universally results in the lift constraint being active, so is a valid solution of equation 2.

All constraints are transformed into the standard form given in equation 1, so the optimization problem

being solved by the optimizer is:

$$
\begin{aligned}
\underset{\boldsymbol{\alpha}\in\Re^D}{\text{minimise}} \quad & C_D \\
\text{subject to} \quad & 0.2625 - C_L \leq 0 \\
& C_{M_x} - 0.1069 \leq 0 \\
& V(\text{initial}) - V \leq 0 \\
& 2.46 - s \leq 0 \\
& s - 3.67 \leq 0 \\
& \\
& 3.0 \leq \alpha_1 \leq 6.0 \\
& -3.12 \leq \alpha_2 \leq 3.12 \\
& 0.06 \leq \alpha_i \leq 0.18 \quad \forall i \in [3, 7] \\
& -0.45 \leq \alpha_i \leq 0.45 \quad \forall i \in [8, 12] \\
& -1 \leq \alpha_i \leq 1 \quad \forall i \in [13, 17] \\
& 0.45 \leq \alpha_i \leq 1.55 \quad \forall i \in [18, 22]
\end{aligned}
\tag{12}
$$

IV. Results

In this section, results of the optimization of the NACA0012 rectangular wing, subject to the optimization problem given in equation 12, are presented. To investigate the modality of the problem, three independent optimization runs were performed. Hence, there are three different initial distribution of particles, which are randomly positioned within the design space. Furthermore, due to the random terms in the optimizer update equations, the stochastic nature of the optimizer means no two runs are repeatable.

The optimizations were run using 48 particles on six 2.6GHz 8-core Intel Sandy Bridge chips for a total of 48 cores (1 per particle). The objective function and constraint evaluations are performed in parallel with one particle assigned to each core. A master core then performs the optimizer update.

The convergence histories of the three runs are given in figure 5. This is an approximate global optimization hence the convergence of the optimizer is restricted, however, it is clear that the optimizer has converged close to a final result, with all three runs only changing by 1 drag count in the final 200 iterations of the maximum run. Trends from the results shown can therefore be extrapolated to more general comments about the problem. It should be noted that all of the three runs have initial drag values above the drag of the baseline wing due to the initial location of the individuals in the global optimization all having (different) values that represent random perturbations to the baseline wing.

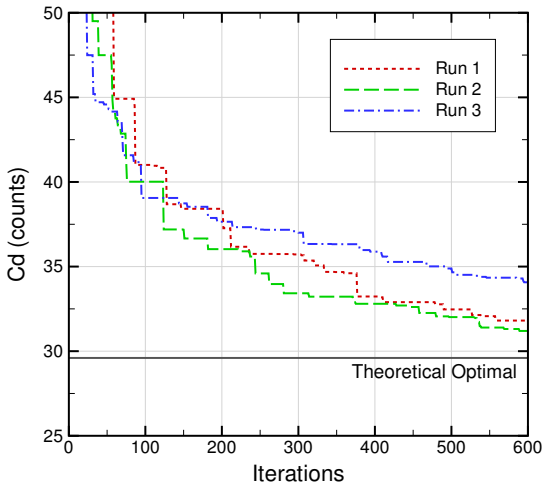

Figure 5: Convergence histories

The optimization results of the three independent runs are shown in table 1. It is first worth noting that the initial solution starts infeasible due to the bending moment constraint being violated (C_{M_x}=0.116 which is slightly higher that the maximum value of 0.1069), however, in all of the final results, this constraint is satisfied. All of the three runs have provided a feasible solution, and this is testament to the high performance of the constrained optimizer used. In terms of active constraints, clearly the lift constraint is active in all cases, as expected, and the area constraint is also active due to the span being calculated to satisfy said constraint. The maximum span constraint is the only other active constraint, which is, again, expected due to the requirement to minimise induced drag. The three runs have resulted in similar drag reductions, each being about a quarter.

Table 1: Optimization results (C_D in counts)

	C_L	C_D	C_{M_x}	V	s	$S/2$	γ	θ	$\Delta J(\%)$	eb^2
Baseline	0.263	43.8	0.116	0.247	3.06	3.02	0.0°	2.99°	-	30.2
Run 1	0.263	31.3	0.105	0.248	3.67	3.02	-0.56°	3.67°	**-28.5%**	42.4
Run 2	0.263	30.7	0.106	0.253	3.67	3.02	-0.50°	3.46°	**-29.9%**	43.3
Run 3	0.263	34.1	0.104	0.252	3.67	3.02	-1.04°	5.09°	**-22.1%**	39.0

The surface shapes and upper surface pressure contours are given in figure 6, and this is clearly where the differences, that are not apparent in the values given in table 1, appear. The spanwise values of the x and z locations of the quarter-chord, the chord length and the thickness are given in more detail in figure 7. All runs have resulted in an almost consistent reduction in chord length along the span, which therefore allows the span to increase in accordance with the requirement to hold the area constant. This is, as noted above to be expected, however the results from run 3 have clearly attempted to reduce the chord as much as possible inboard and shift load inboard at the expense of having a larger, more lightly loaded wing outboard. All runs have had to shift load inboard to satisfy the bending moment constraint, but runs 1 and 2 have resulted in a slightly different approach to run 3.

The profile ($y-z$) views of the runs reveals an interesting trend. While being slightly different in terms of the absolute shapes, all three runs have attempted to produce something akin to a winglet. A substantial change in the profile at about 75% span which all have a similar angle between the profile just preceding the change and the profile just succeeding it. This indicates a similar magnitude of vortex shedding around the 75% spanwise location.

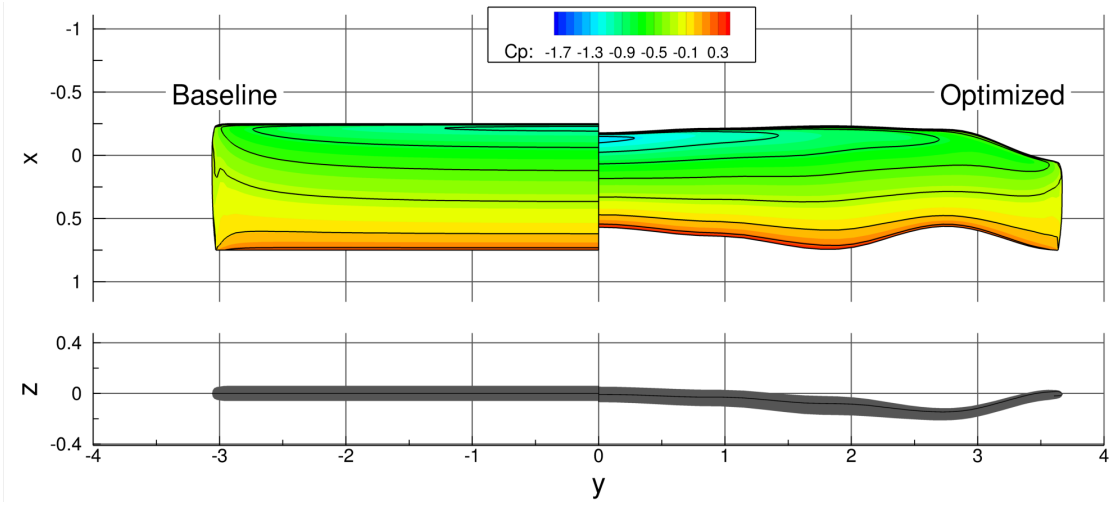

(a) Run 1

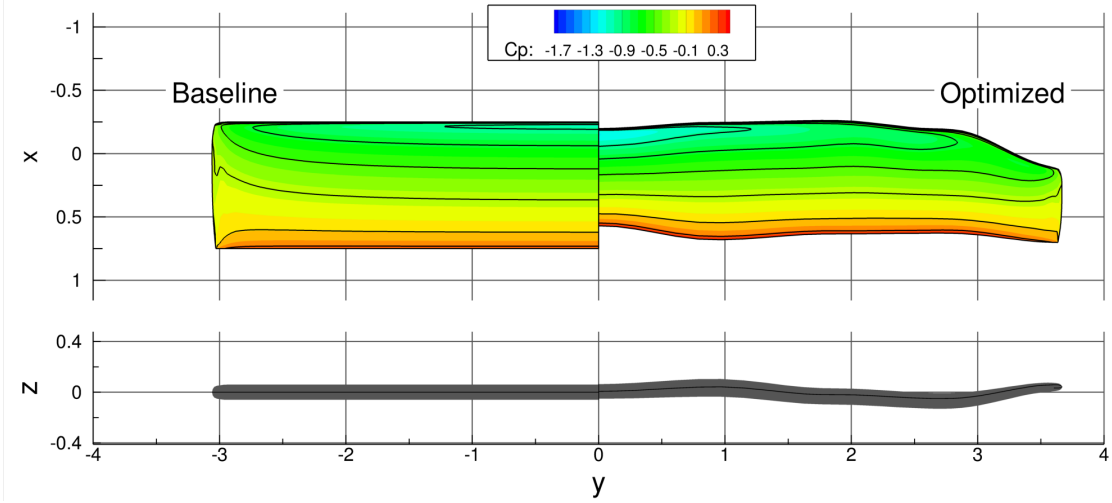

(b) Run 2

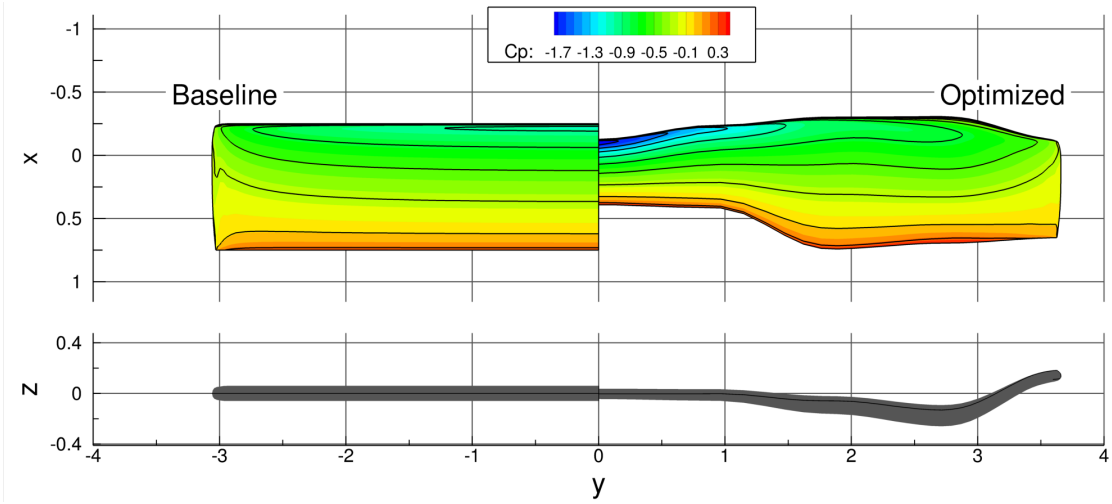

(c) Run 3

Figure 6: Surface shape and upper surface pressure contours

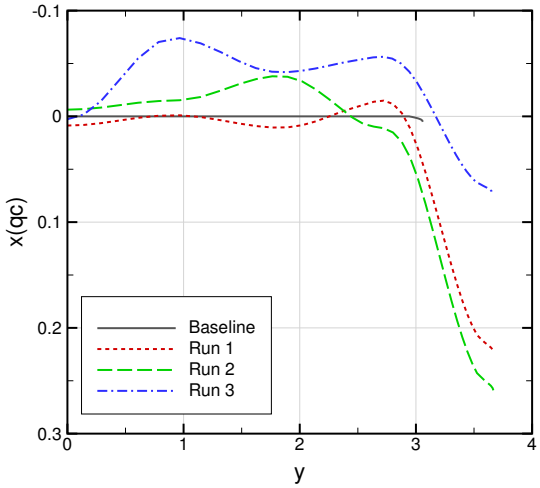

(a) x quarter-chord

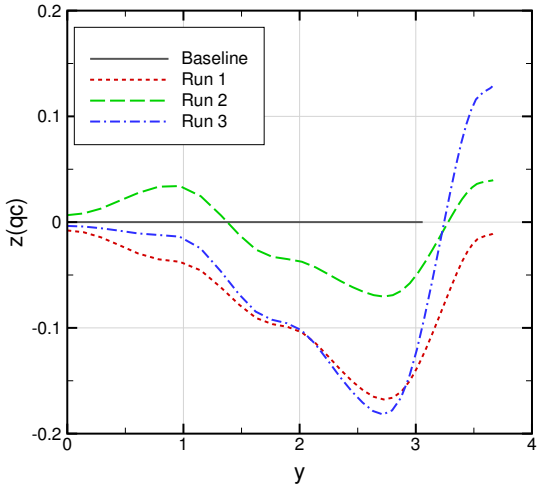

(b) z quarter-chord

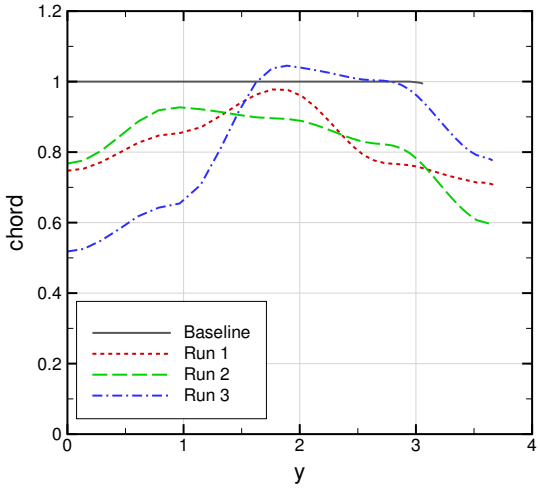

(c) Chord length

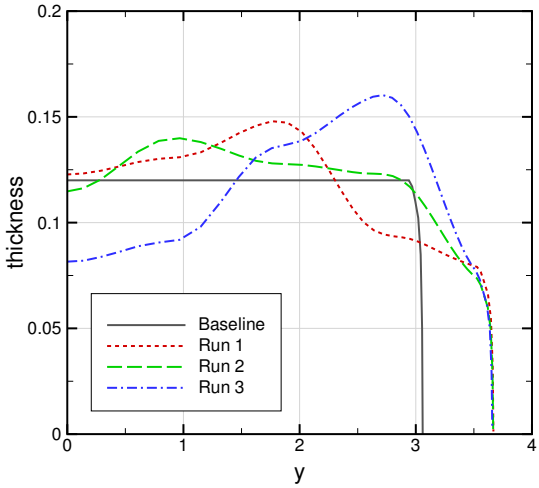

(d) Thickness

Figure 7: Spanwise geometric variations

While the results from the three optimization runs have resulted in substantially different, though showing similar trends, in terms of their shapes, it is also important to consider spanwise loading. The well known optimal loading distribution for a finite span wing is the elliptic profile[47]:

$$\Gamma(\eta) = \Gamma(0)\sqrt{1-\eta^2} \tag{13}$$

where Γ is the circulation and $\eta = y/s$ is the non-dimensional spanwise station. However, with a given lift and bending moment constraint, then the elliptic distribution may not be obtainable, hence the solution of Jones [48] (which is a specific solution of a result later proved by Klein and Viswanathan[49]) becomes the optimal result:

$$\Gamma(\eta) = \Gamma(0)\left[(3-2\epsilon)\sqrt{1-\eta^2} + 6(\epsilon-1)\eta^2 \cosh^{-1}\left(\frac{1}{|\eta|}\right)\right] \tag{14}$$

where:

$$\epsilon = \frac{3\pi}{2}\frac{C_{M_x}}{C_L}$$

A full discussion on optimal loadings subject to bending moment and lift constraints is comprehensively covered by Pate and German [50]. The induced drag can be calculated as:

$$C_{D_i} = \frac{C_L^2}{\pi AR}(1+\delta)$$

where $\delta = 8(\epsilon-1)^2$. For the case considered in this paper, the theoretical minimum induced drag is 29.6 counts, however, due to numerical drag, it is unlikely that this is achievable without fine numerical meshes. Figure 8 gives the initial, elliptic and theoretical optimal result for this case, and compared the three optimization runs with the theoretical optimal result. The bending moment constraint forces an optimal solution with higher inboard wing loading. It is very positive that the optimizations have all resulted in spanwise loadings that are close to optimal. Even though the planforms and profiles are different for all of the results, the loadings are remarkably similar.

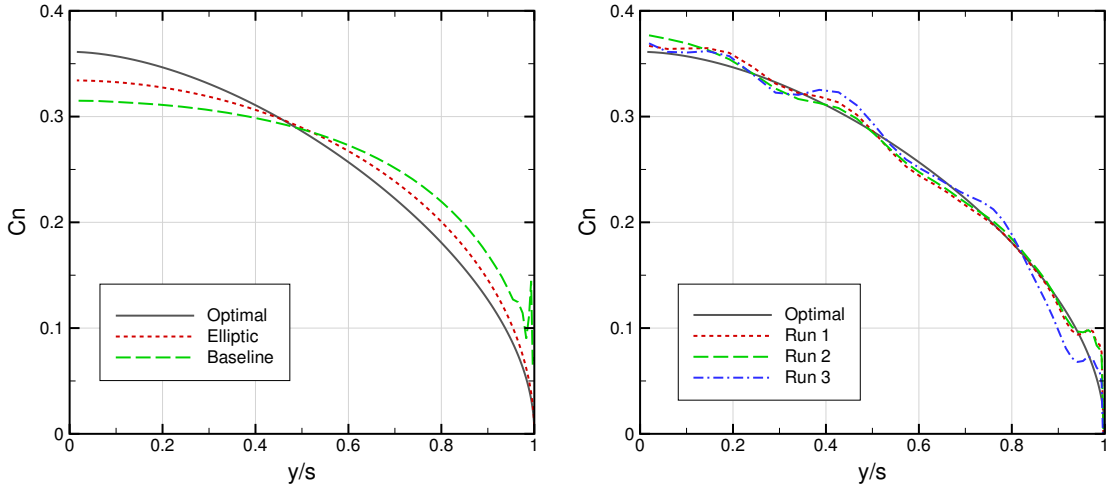

Figure 8: Spanwise load distributions

Surface pressure coefficients at different spanwise stations are given in figure 9, which clearly show that for case 3, there is a high inboard pressure, however, due to the smaller chord, the loading is very similar to the other three cases. The implications for the multimodality of this problem therefore likely depends on the trade-off of chord and loading to force a spanwise loading that is close to optimal. From the spanwise load analysis presented above, there is a theoretical minimum value, however, it is clear from the runs shown here, that there are a number of different ways in which to obtain that minimum value that include vastly different shape changes. This either indicates the presence of multiple, individual optima, or more likely, a flat region of the design space where any variation in the local chord that can produce the optimal loading

distribution. This is analogous in nature to the minimum drag solution of an aerofoil in transonic flow, where the optimum region is the design space is a large, flat region where any aerofoil shape that eliminates a shock and therefore minimise drag due to d'Alembert's paradox, but can still leave an oscillatory surface.

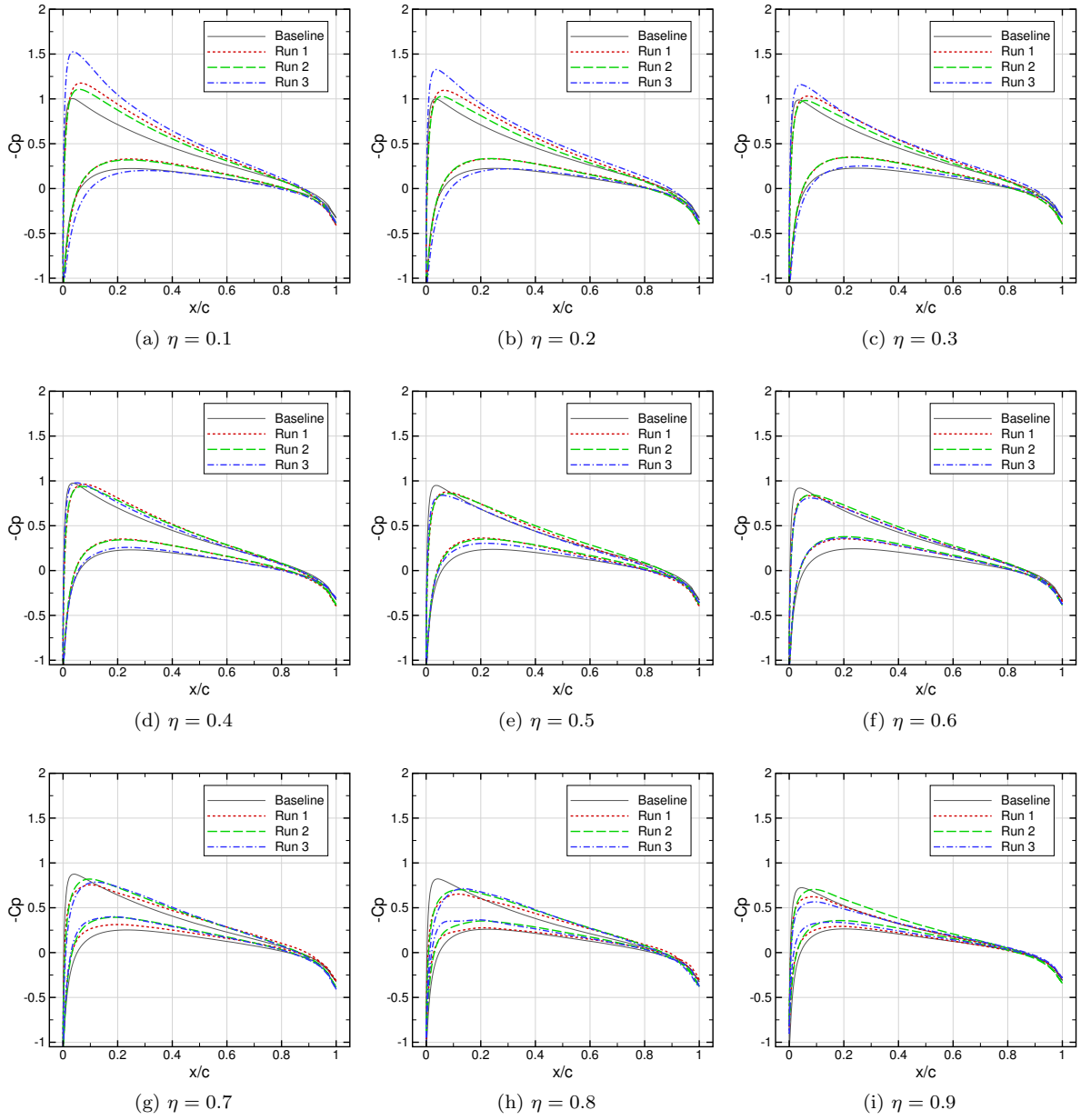

(a) $\eta = 0.1$ (b) $\eta = 0.2$ (c) $\eta = 0.3$

(d) $\eta = 0.4$ (e) $\eta = 0.5$ (f) $\eta = 0.6$

(g) $\eta = 0.7$ (h) $\eta = 0.8$ (i) $\eta = 0.9$

Figure 9: Surface pressure coefficients at spanwise locations

V. Conclusions

An investigation on a new ADODG optimization benchmark case has been performed. The problem, which involves drag minimization of a rectangular NACA0012 wing subject to lift and root-bending moment constraints as well as other geometric constraints, such as span and wing area, is believed to exhibit multimodality. In this work, a constrained global optimizer has been used to optimize the wing, with design variables characterised using a hierarchical control point approach to allow an efficient representation of the wing.

The optimizer, which is a global population-based algorithm (a hybrid of particle swarm optimization and gravitational search algorithm) has been run three times, with each run being independent of the others. Hence, the starting location of the particles in each of the three runs are distinctive. Furthermore, the global optimizer is stochastic and encourages a balance between design space exploration and optima exploitation. A coarse-convergence has been used to reduce run-time while still allowing exploration of the optimizer.

The optima found from each of the three runs have resulted in feasible solutions and are close to the theoretical minimum drag value. All optimal wings have gone to the maximum allowable span, and each have satisfied the lift and wing area equality constraints of the problem. However, while the headline force coefficient values appear similar, the wing shapes exhibit substantial differences, with two of the wings showing similar (relatively uniform) chord distributions, while the other showing much smaller inboard chord. Despite this, the loadings of all three wings are similar. This, possibly, points to the existence of a flat region of the design space where different chord distributions, that result in the same loading, are all optimal.

Acknowledgements

The authors kindly acknowledge the support of the University of Bristol EPSRC Doctoral Training Grant and the University of Bristol Alumni Foundation. This work was carried out using the computational facilities of the Advanced Computing Research Centre, University of Bristol - http://www.bris.ac.uk/acrc/.

References

[1] Poole, D. J., Allen, C. B., and Rendall, T. C. S., "High-fidelity aerodynamic shape optimization using efficient orthogonal modal design variables with a constrained global optimizer," *Computers & Fluids*, Vol. 143, 2017, pp. 1–15.

[2] Poole, D. J., Allen, C. B., and Rendall, T. C. S., "Objective Function and Constraints for Robust Transonic Aerofoil Optimization," *58th AIAA/ASCE/AHS/ASC Structures, Structural Dynamics, and Materials Conference*, Dallas, Texas, 2017, AIAA Paper 2017-0360.

[3] Hicks, R. M. and Henne, P. A., "Wing Design by Numerical Optimization," *Journal of Aircraft*, Vol. 15, No. 7, 1978, pp. 407–412.

[4] Qin, N., Vavalle, A., Le Moigne, A., Laban, M., Hackett, K., and Weinerfelt, P., "Aerodynamic Considerations of Blended Wing Body Aircraft," *Progress in Aerospace Sciences*, Vol. 40, No. 6, 2004, pp. 321–343.

[5] Nielsen, E. J., Lee-Rausch, E. M., and Jones, W. T., "Adjoint Based Design of Rotors in a Noninertial Frame," *Journal of Aircraft*, Vol. 47, No. 2, 2010, pp. 638–646.

[6] Lyu, Z., Kenway, G. K. W., and Martins, J. R. R. A., "Aerodynamic Shape Optimization Investigations of the Common Research Model Wing Benchmark," *AIAA Journal*, Vol. 53, No. 4, 2015, pp. 968–985.

[7] Choi, S., Lee, K. H., Potsdam, M., and Alonso, J. J., "Helicopter Rotor Design Using a Time-Spectral and Adjoint Based Method," *Journal of Aircraft*, Vol. 51, No. 2, 2014, pp. 412–423.

[8] Morris, A. M., Allen, C. B., and Rendall, T. C. S., "CFD-based Optimization of Aerofoils Using Radial Basis Functions for Domain Element Parameterization and Mesh Deformation," *International Journal for Numerical Methods in Fluids*, Vol. 58, No. 8, 2008, pp. 827–860.

[9] Allen, C. B. and Rendall, T. C. S., "Computational-Fluid-Dynamics-Based Optimisation of Hovering Rotors Using Radial Basis Functions for Shape Parameterisation and Mesh Deformation," *Optimization and Engineering*, Vol. 14, 2013, pp. 97–118.

[10] Masters, D. A., Taylor, N. J., Rendall, T. C. S., Allen, C. B., and Poole, D. J., "Geometric Comparison of Aerofoil Shape Parameterization Methods," *AIAA Journal*, 2017, Published online.

[11] Chernukhin, O. and Zingg, D. W., "Multimodality and Global Optimization in Aerodynamic Design," *AIAA Journal*, Vol. 51, No. 6, 2013, pp. 1342–1354.

[12] Lyu, Z., Xu, Z., and Martins, J. R. R. A., "Benchmarking Optimization Algorithms for Wing Aerodynamic Design Optimization," *Eighth International Conference on Computational Fluid Dynamics (ICCFD8)*, Chegdu, China, 2014, ICCFD8-2014-0203.

[13] Bisson, F. and Nadarajah, S. K., "Adjoint-Based Aerodynamic Optimization of Benchmark Problems," *53rd AIAA Aerospace Sciences Meeting*, Kissimmee, Florida, 2015, AIAA Paper 2015-1948.

[14] Poole, D. J., Allen, C. B., and Rendall, T. C. S., "Control Point-Based Aerodynamic Shape Optimization Applied to AIAA ADODG Test Cases," *53rd AIAA Aerospace Sciences Meeting*, Kissimmee, Florida, 2015, AIAA Paper 2015-1947.

[15] Meheut, M., Destarac, D., Carrier, G., Anderson, G., Nadarajah, S., Poole, D., Vassberg, J., and Zingg, D., "Gradient-Based Single and Multi-points Aerodynamic Optimizations with the elsA Software," *53rd AIAA Aerospace Sciences Meeting*, Kissimmee, Florida, 2015, AIAA Paper 2015-0263.

[16] Lee, C., Koo, D., Telidetzki, K., Buckley, H. P., Gagnon, H., and Zingg, D. W., "Aerodynamic Shape Optimization of Benchmark Problems Using Jetstream," *53rd AIAA Aerospace Sciences Meeting*, Orlando, Florida, 2015, AIAA Paper 2015-0262.

[17] LeDoux, S. T., Vassberg, J. C., Young, D. P., Fugal, S., Kamenetskiy, D., Huffman, W. P., Melvin, R. G., and Smith, M. F., "Study Based on the AIAA Aerodynamic Design Optimization Discussion Group Test Cases," *AIAA Journal*, Vol. 53, No. 7, 2015, pp. 1910–1935.

[18] Kenway, G. K. W. and Martins, J. R. R. A., "Multipoint Aerodynamic Shape Optimization Investigations of the Common Research Model Wing," *AIAA Journal*, Vol. 54, No. 1, 2016, pp. 113–128.

[19] Masters, D. A., Poole, D. J., Taylor, N. J., Rendall, T. C. S., and Allen, C. B., "Impact of Shape Parameterisation on Aerodynamic Optimisation of Benchmark Problem," *54th AIAA Aerospace Sciences Meeting*, San Diego, California, 2016, AIAA Paper 2016-1544.

[20] Masters, D. A., Poole, D. J., Taylor, N. J., Rendall, T. C. S., and Allen, C. B., "Influence of Shape Parameterisation on a Benchmark Aerodynamic Optimisation Problem," *Journal of Aircraft*, 2017, In print.

[21] Zingg, D. W. and Streuber, G., "Aerodynamic Design Optimization Workshop: Multimodal Subsonic Inviscid Optimization Problem," Tech. rep., AIAA ADODG, 2017, https://info.aiaa.org/tac/ASG/APATC/AeroDesignOpt-DG/Test%20Cases/ADODG%20Case%206%20Multimodal%20Subsonic%20Inviscid%20Optimization.pdf.

[22] Holland, J. H., *Adaptation in Natural and Artificial Systems*, The University of Michigan Press, 1975.

[23] Storn, R. and Price, K., "Differential Evolution - A simple and efficient adaptive scheme for global optimization over continuous spaces," Tech. rep., ICSI, UC Berkeley, 1995, TR-95-012.

[24] Storn, R. and Price, K., "Differential Evolution A Simple and Efficient Heuristic for Global Optimization over Continuous Spaces," *Journal of Global Optimization*, Vol. 11, 1997, pp. 341–359.

[25] Kennedy, J. and Eberhart, R., "Particle Swarm Optimization," *1995 IEEE International Conference on Neural Networks*, Perth, Australia, 1995.

[26] Colorni, A., Dorigo, M., and Maniezzo, V., "Distributed Optimization by Ant Colonies," *European Conference on Artificial Life*, Paris, France, 1991.

[27] Rashedi, E., Nezamabadi-pour, H., and Saryazdi, S., "GSA: A Gravitational Search Algorithm," *Information Sciences*, Vol. 179, 2009, pp. 2232–2248.

[28] Zingg, D. W., Nemec, M., and Pulliam, T. H., "A Comparative Evaluation of Genetic and Gradient-based Algorithms Applied to Aerodynamic Optimization," *European Journal of Computational Mechanics*, Vol. 17, 2008, pp. 103–126.

[29] Namgoong, H., Crossley, W., and Lyrintzis, A. S., "Global Optimization Issues for Transonic Airfoil Design," *9th AIAA/ISSMO Symposium on Multidisciplinary Analysis and Optimization*, Atlanta, Georgia, 2002, AIAA Paper 2002-5641.

[30] Khurana, M. S., Winarto, H., and Sinha, A. K., "Airfoil Optimisation by Swarm Algorithm with Mutation and Artificial Neural Networks," *47th AIAA Aerospace Sciences Meeting Including the New Horizons Forum and Aerospace Exposition*, Orlando, Florida, 2010, AIAA Paper 2009-1278.

[31] Payot, A. D. J., Rendall, T. C. S., and Allen, C. B., "Restricted Snakes: a Flexible Topology Parameterisation Method for Aerodynamic Optimisation," *55th AIAA Aerospace Sciences Meeting*, Dallas, Texas, 2017, AIAA Paper 2017-1410.

[32] Mukesh, R., Pandiyarajan, R., Selvakumar, U., and Lingadurai, K., "Influence of Search Algorithms on Aerodynamic Design Optimisation of Aircraft Wings," *Procedia Engineering*, Vol. 38, 2012, pp. 2155–2163.

[33] de Falco, I., Della Cioppa, A., Iazzetta, A., and Tarantino, E., "Evolutionary Algorithms for Aerofoil Design," *International Journal of Computational Fluid Dynamics*, Vol. 11, No. 1-2, 1998, pp. 51–77.

[34] Jahangirian, A. and Shahrokhi, A., "Aerodynamic Shape Optimization Using Efficient Evolutionary Algorithms and Unstructured CFD Solver," *Computers and Fluids*, Vol. 46, 2011, pp. 270–276.

[35] Giannakoglou, K. C., "Design of Optimal Aerodynamic Shapes Using Stochastic Optimization Methods and Computational Intelligence," *Progress in Aerospace Sciences*, Vol. 38, 2002, pp. 43–76.

[36] Epstein, B. and Peigin, S., "Optimization of 3D Wings Based on Navier-Stokes Solutions and Genetic Algorithms," *International Journal of Computational Fluid Dynamics*, Vol. 20, No. 2, 2006, pp. 75–92.

[37] Poole, D. J., Allen, C. B., and Rendall, T. C. S., "A Generic Framework for Handling Constraints with Agent-Based Optimization Algorithms and Application to Aerodynamic Design," *Optimization and Engineering*, 2016, Published online.

[38] Jameson, A., Schmidt, W., and Turkel, E., "Numerical solution of the Euler equations by finite volume methods using Runge Kutta time stepping schemes," *14th Fluid and Plasma Dynamics Conference*, Palo Alto, California, 1981, AIAA Paper 1981-1259.

[39] Allen, C. B., "Multigrid Convergence of Inviscid Fixed- and Rotary-Wing Flows," *International Journal for Numerical Methods in Fluids*, Vol. 39, No. 2, 2002, pp. 121–140.

[40] Allen, C. B., "Towards Automatic Structured Multiblock Mesh Generation using Improved Transfinite Interpolation," *International Journal for Numerical Methods in Engineering*, Vol. 74, No. 5, 2008, pp. 697–733.

[41] Morris, A. M., Allen, C. B., and Rendall, T. C. S., "Domain-Element Method for Aerodynamic Shape Optimization Applied to a Modern Transport Wing," *AIAA Journal*, Vol. 47, No. 7, 2009, pp. 1647–1659.

[42] Rendall, T. C. S. and Allen, C. B., "Unified Fluid-Structure Interpolation and Mesh Motion Using Radial Basis Functions," *International Journal for Numerical Methods in Engineering*, Vol. 74, No. 10, 2008, pp. 1519–1559.

[43] Rendall, T. C. S. and Allen, C. B., "Efficient Mesh Motion Using Radial Basis Functions with Data Reduction Algorithms," *Journal of Computational Physics*, Vol. 228, No. 17, 2009, pp. 6231–6249.

[44] Wendland, H., *Scattered Data Approximation*, Cambridge University Press, 1st ed., 2005.

[45] Allen, C. B., Poole, D. J., and Rendall, T. C. S., "Efficient Modal Design Variables Applied to Aerodynamic Optimization of a Modern Transport Wing," *17th AIAA/ISSMO Multidisciplinary Analysis and Optimization Conference*, Washington, D.C., 2016, AIAA Paper 2016-3215.

[46] Deb, K., "An Efficient Constraint Handling Method for Genetic Algorithms," *Computer Methods in Applied Mechanics and Engineering*, Vol. 186, 2000, pp. 311–338.

[47] Prandtl, L., "Applications of Modern Hydrodynamics to Aeronautics," Tech. rep., NACA, 1923, NACA Report 116.

[48] Jones, R. T., "The Spanwise Distribution of Lift for Minimum Induced Drag of Wings Having a Given Lift and a Given Bending Moment," Tech. rep., NACA, 1950, NACA Report 2249.

[49] Klein, A. and Viswanathan, S. P., "Approximate Solution for Minimum Induced Drag of Wings with Given Structural Weight," *Journal of Aircraft*, Vol. 12, No. 2, 1975, pp. 124–126.

[50] Pate, D. J. and German, B. J., "Lift Distributions for Minimum Induced Drag with Generalized Bending Moment Constraints," *Journal of Aircraft*, Vol. 50, No. 3, 2013, pp. 936–946.